
Relaxing Equivariance Constraints with Non-stationary Continuous Filters

Tycho F.A. van der Ouderaa
Imperial College London
United Kingdom

David W. Romero
Vrije Universiteit Amsterdam
The Netherlands

Mark van der Wilk
Imperial College London
United Kingdom

Abstract

Equivariances provide useful inductive biases in neural network modeling, with the translation equivariance of convolutional neural networks being a canonical example. Equivariances can be embedded in architectures through weight-sharing and place symmetry constraints on the functions a neural network can represent. The type of symmetry is typically fixed and has to be chosen in advance. Although some tasks are inherently equivariant, many tasks do not strictly follow such symmetries. In such cases, equivariance constraints can be overly restrictive. In this work, we propose a parameter-efficient relaxation of equivariance that can effectively interpolate between a (i) non-equivariant linear product, (ii) a strict-equivariant convolution, and (iii) a strictly-invariant mapping. The proposed parameterisation can be thought of as a building block to allow adjustable symmetry structure in neural networks. In addition, we demonstrate that the amount of equivariance can be learned from the training data using backpropagation. Gradient-based learning of equivariance achieves similar or improved performance compared to the best value found by cross-validation and outperforms baselines with partial or strict equivariance on CIFAR-10 and CIFAR-100 image classification tasks.

1 Introduction

Symmetric properties, such as equivariances and invariances, can be embedded into neural network architectures to provide inductive biases that leads to better data-efficiency and improved generalisation. Convolutional layers are known to provide translation equivariance in simple Euclidean spaces, and recent works have allowed various extensions to more complex groups and domains. However, symmetries are typically fixed, must be specified in advance, and can not be adjusted.

Symmetries embedded in network architectures enforce a hard constraint on the functions a neural network can represent. This can be an effective way to encode prior knowledge for problems that are inherently symmetric. However, hard symmetry constraints can become prohibitive if a problem does not strictly follow the symmetries. For example, convolutional layers can not encode potentially relevant absolute positional information, and ‘6’s and a ‘9’s become difficult to distinguish under rotation invariance. Relaxed symmetry constraints can mitigate such potential symmetry misspecification without losing the useful inductive biases that symmetries provide.

We propose to relax equivariance constraints by generalising the convolution operator with non-stationary filters that can also depend on absolute group elements. This results in a layer that can efficiently interpolate between (i) non-invariant linear products akin to a fully-connected layer, (ii) strict group equivariant convolutions, and (iii) strict group invariant mappings (Fig. 1).

The importance of this work is twofold. First of all, relaxable symmetry constraints can directly improve the performance in cases where strict symmetries are misspecified and result in an overly restrictive model class. Secondly, automatically learning symmetry structure from data is an interesting problem. Work in this field often focuses on invariances [34, 4, 33, 29, 12], which are easier to parameterise than equivariances. We show a way to effectively parameterise learnable equivariance constraints and demonstrate gradient-based learning of layer-by-layer equivariance constraints.

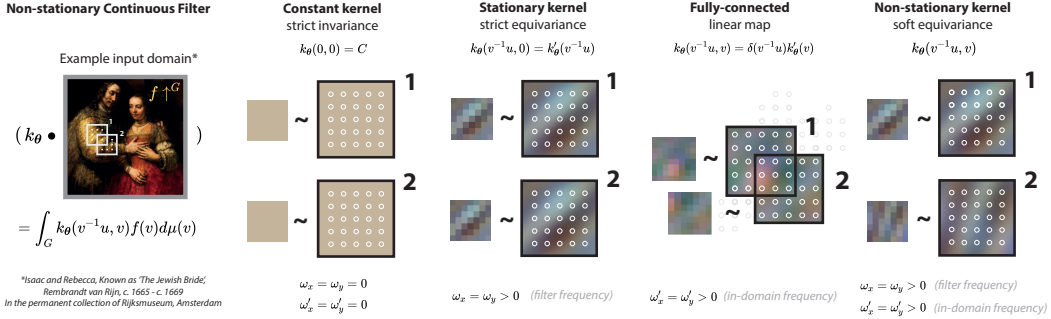


Figure 1: The non-stationary integral operator. Strict invariance, strict equivariance, non-equivariance, and relaxed equivariance are all special cases that depend on the frequency parameters ω and ω' . The case of the translation group $G=\mathbb{T}(2)$ is illustrated: unlike the regular convolution with stationary kernels, the proposed non-stationary filter can depend on the position where it is applied.

2 Related Work

Group equivariance. Equivariance constraints applied to layers provide a strong inductive bias that enforce transformations in the input to result in equivalent transformations in the output. For compact groups it can be shown that this constraint naturally leads to (group) convolutions [15]. Many works have allowed for equivariances to groups other than translation, including continuous roto-translations [38, 36, 16], discrete roto-translations [5, 3], scale [37], and permutations [39] and non-Euclidean domains, such as spheres [6], points clouds [10] and graphs [27].

Symmetry misspecification and approximate equivariance. Although symmetry constraints can be very effective in machine learning, they can become prohibitive if data does not exactly follow the enforced symmetry. For instance, Liu et al. [17] raised an ‘intriguing failing’ of convolutional neural networks by showing that they can not encode absolute coordinate information. Adding explicit coordinate information was proposed as an ad-hoc solution to the problem, effectively breaking strict equivariance constraints. To achieve the same result, Finzi et al. [8] proposed to break equivariance of a convolutional layer by summing it with a non-equivariant fully-connected layer, requiring many additional parameters. Alternatively, Romero and Lohit [24] consider a sparse local support around the group identity element to break equivariance. This is effective for sparsely sampled subgroups, such as rotation, but becomes less practical for more densely sampled groups such as translation where the local support could lead to very sparse feature maps. Lastly, Wang et al. [35] propose a relaxed convolutional operator similar to our non-stationary approach, but require a low-rank factorisation which potentially limits the expressivity of the feature maps. The same work briefly discusses a mathematical description without such factorisation similar to our proposal which is deemed “too large a trainable weight space to be practical”. This is true for discrete convolutional kernels. Instead we define our kernels as continuous kernels [26] parameterised with a finite number of parameters. Consequently, our weight space becomes tractable and does not pose a problem at all.

Physics and filtering. Symmetries play a central role in physics. In [35] approximate equivariances are used to allow more robust models for dynamical systems. In Noether networks [1] conservation laws are inferred by learning symmetries from data. Our work could offer new insights in how symmetry constraints could be relaxed in such applications. In geophysics and seismology, there are some interesting parallels between non-stationary filtering methods and approximate equivariances in machine learning. In particular, [19] discusses generalisations of the convolution in the context of non-stationary filtering very similar to how we propose to relax equivariances in neural networks.

Automatic symmetry discovery. Automatically inferring symmetry structure of neural network architectures from data is an interesting open problem. For instance, Lorraine et al. [18] learn data augmentations by differentiating the validation loss using the implicit function theorem and Zhou et al. [40] showed how symmetry structure could be learned through a meta-learning outer loop. In

[4] and [8] symmetries are selected using a training loss directly, using an additional regulariser. Symmetry discovery methods often focus on learning global invariances [34, 4, 29, 33, 12], which are easier to parameterise compared to layer-wise equivariences. We propose a way to continuously relax equivariences allowing efficient parameterisation of learnable equivariance for symmetry discovery methods. Inspired by the regularisation used in [4] to learn augmented inputs, we demonstrate that our parameterisation can be used for gradient-based learning of equivariance in each layer from data.

3 Background

3.1 Groups

A Lie group provides a natural way to describe continuous symmetry, as it forms a continuous manifold of which underlying elements are equipped with a group structure. Lie groups do not necessarily form a vector space. However, to every Lie group G we can associate an underlying vector space called the Lie algebra \mathfrak{g} . The Lie algebra corresponds to the tangent space of the group at the identity, has the same dimensionality as the group, and captures the local structure of the group. Because the Lie algebra is a vector space, elements $\mathbf{a} \in \mathfrak{g}$ can be expanded in a basis in the Lie algebra $\mathbf{a} = \sum_{i=1}^{\dim(G)} \alpha_i A_i$ with coefficients $\alpha \in \mathbb{R}^{\dim(G)}$. The exponential map $\exp : \mathfrak{g} \rightarrow G$ maps elements from the Lie algebra to the Lie group. We can also define a logarithm $\log : G \rightarrow \mathfrak{g}$ map from the Lie group to the Lie algebra. Such a choice always exists, but is not necessarily smooth or unique.

3.2 Equivariance and invariance

Equivariance is the property of a mapping such that transformations to the input result in equivalent transformations to the output. If changes are invertible, they can be described as the action of a group G on some space \mathcal{X} . Formally, we say that a function $h : \mathcal{X} \rightarrow \mathcal{X}$ is *equivariant to the group G* if $h(g \cdot x) = g \cdot h(x)$ for all $g \in G, x \in \mathcal{X}$.

If the output of the function is completely independent to the action of the group G on the input, we say that the function is *invariant to the group G* . Formally, a function $h : \mathcal{X} \rightarrow \mathcal{X}$ is *invariant to the group G* if $h(g \cdot x) = h(x)$ for all $g \in G, x \in \mathcal{X}$.

3.3 The group convolution

Let $f : G \rightarrow \mathbb{R}$ be an input signal and $k_\theta : G \rightarrow \mathbb{R}$ be a convolutional kernel parameterised by θ . The group convolution is defined as:

$$h(u) = (k_\theta \star f)(u) = \int_G k_\theta(v^{-1}u) f(v) d\mu(v), \quad (1)$$

where we integrate with respect to the Haar measure of the group μ . Group convolutional structure is not just a sufficient, but also a necessary condition for equivariance to the action of a compact group [15]. The regular convolution for translation equivariance is the special case where the group is the translation group $G = \text{T}(n) \cong \mathbb{R}^n$, and the group action is given by addition, i.e., $v^{-1}u = u - v$.

The convolutional kernel $k_\theta(v^{-1}u)$, which we will sometimes refer to as ‘filter’ for stylistic purposes, is called *stationary* because it can only depend on u and v through $v^{-1}u$. This invariance of the kernel is an important constraint and in fact a requirement for h to be *equivariant*. Breaking the stationarity of the kernel allows us to relax the equivariant symmetry constraints, which is one of the central ideas of this paper.

3.4 Group lifting

The input and output signals of a neural network are typically not defined on the group G , but rather on an input and output space \mathcal{X} and \mathcal{Y} . Using a group lifting and projection procedure [15, 7], we can define our model on the group and still apply it on the input and output space. We define a lifting operator \uparrow^G to map input signals $f : \mathcal{X} \rightarrow \mathbb{R}$ to functions on the group $f \uparrow^G : G \rightarrow \mathbb{R}$. Similarly, we define a projection operator that maps function on the group $f' : G \rightarrow \mathbb{R}$ to functions on the output space $f' \downarrow_{\mathcal{Y}} : \mathcal{Y} \rightarrow \mathbb{R}$.

4 Method

4.1 Non-stationary Integral Operator

The group convolution operation of Eq. (1) is strictly equivariant due to the stationarity of the kernel. That is, the kernel k only depends on relative group element $v^{-1}u$. For translation $G=\mathbb{T}(2)$, the kernel only depends on relative coordinates $(u - v)$ and not on the absolute position in the image. To relax equivariance constraints, we let the kernel also depend on the absolute group element v :

$$h(u) = (k_{\theta} \bullet f)(u) = \int_G k_{\theta}(v^{-1}u, v)f(v)d\mu(v). \quad (2)$$

The main difference with the group convolution of Eq. (1) is that the kernel $k_{\theta} : G \times G \rightarrow \mathbb{R}$ now has two input group elements. We will refer to the first input argument $v^{-1}u \in G$ as the *stationary component* and the second input argument $v \in G$ as the *non-stationary component*. In case of translation, this change lets the kernels depend also on the absolute coordinate of the input image on which it is applied. Consequently, $h(u)$ does no longer describe the regular convolution, but rather a non-stationary integral operator, for which the convolution remains a limiting case.

For the purpose of this work, there is no meaningful difference between expressing the non-stationary component in the input domain $k_{\theta}(v^{-1}u, v)$ or the output domain $k_{\theta}(v^{-1}u, u)$. For consistency, we will stick with the input domain throughout this work. One could also think of writing the kernel in an even more general form: $k_{\theta}(u, v)$. This, as such, does not lead to a more expressive kernel in the sense that both forms can represent the same class of functions (for a proof, see App. B.1). Further, in this more general way of writing the non-stationary kernel it will become harder to formulate a parameterisation that allows for controllable symmetry constraints, so we do not consider it.

The non-stationary integral operator of Section 4.1 can represent interesting special cases through an independence of k_{θ} with respect to the first and second input arguments.

Remark 1 (Linear product / Fully-connected). *If the kernel equals an impulse response in the stationary component multiplied by some function k'_{θ} in the non-stationary component $k_{\theta}(v^{-1}u, v) = \delta(v^{-1}u)k'_{\theta}(v)$, then the operator $h(u) = (k_{\theta} \bullet f)(u)$ corresponds to a linear product with k'_{θ} .*

If we have a kernel $k_{\theta}(v^{-1}u, v) = \delta(v^{-1}u)k'_{\theta}(v)$, then we have that:

$$h_{\theta}(u) = \int_G k_{\theta}(v^{-1}u, v)f(v)d\mu(v) = \int_G \delta(v^{-1}u)k'_{\theta}(v)f(v)d\mu(v) = k'_{\theta}(u)f(u), \quad (3)$$

which is the linear product between $k'_{\theta}(u)$ and input $f(u)$. This is akin to an element-wise product continuously defined on G . Optionally, this could be followed by an invariant layer to average pool activations. If the operation is performed over channels and we regard these as output features, this corresponds to a fully-connected layer in the discrete case $G=\mathbb{Z}^n$, with weights given by all k'_{θ} .

Remark 2 (Group equivariance / Convolution). *If the kernel does not depend on the non-stationary component, then the operator $h(u) = (k_{\theta} \bullet f)(u)$ is equivalent to a strict G -equivariant convolution.*

If the kernel only depends on the first stationary component, then $k_{\theta}(v^{-1}u, v) = k'_{\theta}(v^{-1}u)$, and:

$$h_{\theta}(u) = \int_G k_{\theta}(v^{-1}u, v)f(v)d\mu(v) = \int_G k'_{\theta}(v^{-1}u)f(v)d\mu(v) = (k'_{\theta} \star f)(u), \quad (4)$$

which equals the group convolution which is known to be strictly group equivariant.

Remark 3 (Group Invariance / Pooling). *If the kernel is independent of both stationary and non-stationary components, the operator $h(u) = (k_{\theta} \bullet f)(u)$ is strictly G -invariant.*

If the kernel does not depend on both inputs, it must be constant $k_{\theta}(v^{-1}u, u) = C$, and we obtain:

$$h_{\theta}(u) = \int_G k_{\theta}(v^{-1}u, u)f(v)d\mu(v) = C' \int_G f(v)d\mu(v), \quad (5)$$

which is a scaled average ‘global-pooling’ over group actions and leads to strict group invariance. We obtain partial invariance or ‘local-pooling’ if the kernel is only non-zero constant in some local support of the stationary domain.

4.2 Parameterising the kernel

Lie algebra basis. In Eq. (2), we have proposed a non-stationary integral operator with a kernel $k_\theta : G \times G \rightarrow \mathbb{R}$ that takes two input arguments: the stationary group element $v^{-1}u$ and a non-stationary group element v . We can parameterise the kernel k_θ in terms of real vector spaces, which are more practical to work with, by defining elements in an explicit Lie algebra basis. To do so, we first define a logarithm function \log and express the kernel $k = \hat{k}(\log g, \log h)$ in terms of a kernel in the Lie algebra $\hat{k} : \mathfrak{g} \times \mathfrak{g} \rightarrow \mathbb{R}$, which always form vector spaces. For rotation $G=SO(2)$, the exponential map \exp sending Lie algebra elements (on a line) to Lie group elements (on a circle) is not left invertible, but is right invertible, as a function. As the right inverse is not unique, we choose to use the principal log sending Lie group elements to Lie algebra elements closest to the identity. In general, such a choice for the logarithm always exists but is not necessarily unique or continuous. We choose a vector space basis $\{A_i\}_{i=1}^{\dim(G)}$ to express Lie algebra elements $\mathbf{a} \in \mathfrak{g}$ in terms of coefficients $\boldsymbol{\alpha} \in \mathbb{R}^{\dim(G)}$ that relate to Lie group elements $g \in G$ by:

$$g = \exp(\mathbf{a}) = \exp \sum_{i=1}^{\dim(G)} \alpha_i A_i \in G, \quad \boldsymbol{\alpha} \in \mathbb{R}^{\dim(G)} \quad (6)$$

Through this construction, each group element g corresponds through a choice of log to a unique Lie algebra element \mathbf{a} which can be implemented as a real vector $\boldsymbol{\alpha}$.

Functions in the Lie algebra. We parameterise the proposed non-stationary kernel $k_\theta : G \times G \rightarrow \mathbb{R}$, which takes two input arguments, in the Lie algebra kernel $\hat{k} : \mathfrak{g} \times \mathfrak{g} \rightarrow \mathbb{R}$ acting on a product space of two vector spaces. We refer to the first vector space related to the stationary component as the *filter space*, as it corresponds to space in which filters of conventional convolutions are defined. And refer to the second vector space of the non-stationary component as the *domain space*, because elements directly relate to absolute group elements in the input domain.

In Section 4.1 we showed that an independence of the kernel with respect to the first and second input argument correspond to strict equivariant and invariant symmetry constraints. We would, therefore, like to choose \hat{k} such that we can control the dependence on the stationary and non-stationary components, as this will allow for explicit control over symmetry constraints. To do so, we parameterise \hat{k} using a set of random Fourier features [23] with a frequency parameter ω for each dimension. The frequency parameter gives us control over the spectral properties of the function in filter space and domain space. But crucially, a frequency of $\omega=0$ results in a constant infinite lengthscale and therefore a function \hat{k} that is independent to the associated input dimension. This mechanic allows us to select the special cases discussed in Section 4.1 and interpolate between them! Together, we have a frequency parameter $\boldsymbol{\omega} \in \mathbb{R}^{\dim(G)}$ that controls spectral properties in filter space and a frequency parameter $\boldsymbol{\omega}' \in \mathbb{R}^{\dim(G)}$ to control spectral properties in domain space. We propose a weight-space parameterisation that allows for explicit control over the symmetry properties of the layer through frequency parameters $\boldsymbol{\omega}$ and $\boldsymbol{\omega}'$.

Weight-space implementation. We choose to parameterise our kernel in a finite D -dimensional random Fourier features (RFF) [23, 31] basis $\boldsymbol{\gamma}_\omega : \mathfrak{g} \rightarrow \mathbb{R}^{2D}$:

$$\boldsymbol{\gamma}_\omega(\mathbf{a}) = \sqrt{\frac{1}{D}} \begin{bmatrix} \cos(2\pi(\mathbf{W}(\boldsymbol{\alpha} \odot \boldsymbol{\omega}))) \\ \sin(2\pi(\mathbf{W}(\boldsymbol{\alpha} \odot \boldsymbol{\omega}))) \end{bmatrix}. \quad (7)$$

embedding Lie algebra elements $\mathbf{a} \in \mathfrak{g}$ as real vectors using their coefficients $\boldsymbol{\alpha} \in \mathbb{R}^{\dim(G)}$ where the frequency can be explicitly controlled by frequency parameter $\boldsymbol{\omega} \in \mathbb{R}^{\dim(G)}$. Values of $\mathbf{W} \in \mathbb{R}^{D \times \dim(G)}$ are randomly initialised and can be kept fixed. We parameterise the Lie algebra kernel $\hat{k} : \mathfrak{g} \times \mathfrak{g} \rightarrow \mathbb{R}$ with a neural network $\text{NN}_\theta : \mathbb{R}^{4D} \rightarrow \mathbb{R}$ taking concatenated Fourier features as input:

$$\hat{k}_\theta(\mathbf{a}_{v^{-1}u}, \mathbf{a}_v) = \text{NN}_\theta \left(\begin{bmatrix} \boldsymbol{\gamma}_\omega(\mathbf{a}_{v^{-1}u}) \\ \boldsymbol{\gamma}_{\omega'}(\mathbf{a}_v) \end{bmatrix} \right) \quad (8)$$

where $\boldsymbol{\gamma}_\omega(\mathbf{a}_{v^{-1}u})$ are the Fourier features on the filter space and $\boldsymbol{\gamma}_{\omega'}(\mathbf{a}_v)$ are the Fourier features on the domain space, respectively parameterised by $\boldsymbol{\omega}$ and $\boldsymbol{\omega}'$ frequency parameter vectors.

Directly representing the kernel with an MLP on $\boldsymbol{\alpha}$ without Fourier features will likely hamper performance as MLPs are known to suffer from ‘spectral bias’ [2, 22], making it difficult to encode

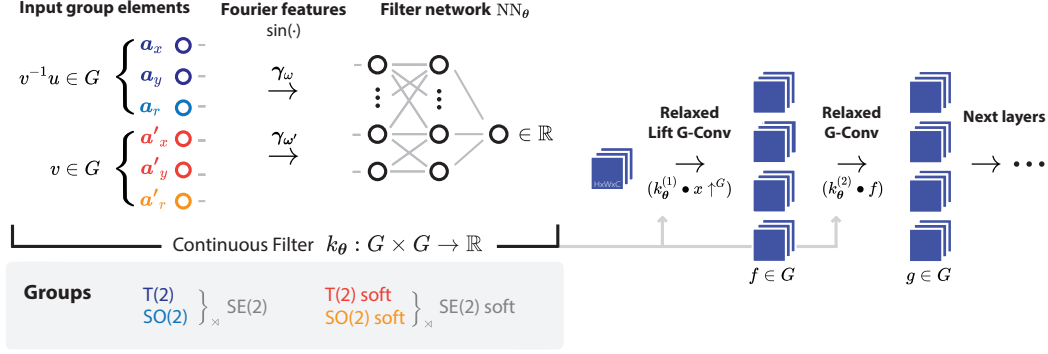


Figure 2: Parameterisation of continuous filter k_θ in soft-SE(2) equivariant model. Fourier features γ_ω and $\gamma_{\omega'}$ represent the stationary and non-stationary input components $v^{-1}u \in G$ and $v \in G$. Frequency parameters ω and ω' respectively control the spectra of the filter space and domain space, generalising the convolution to an operator with continuously adjustable symmetry constraints.

high-frequency functions. Sinusoidal activations in random Fourier features [23, 31] and SIRENs [30] alleviate this issue and have been found suitable encodings of positional information in neural networks [32], including (place-coded) continuous kernels in neural networks [26, 25].

Intuition behind frequency parameters. The frequency parameters ω and ω' control the frequencies in the respective ‘filter space’ and ‘domain space’. Specific values of ω and ω' correspond to a layer h that exactly is or interpolates between special cases discussed in Section 4.1. Most notably, for $\omega' = \mathbf{0}$ the layer becomes a strictly equivariant convolution and for both $\omega = \omega' = \mathbf{0}$ the layer performs invariant pooling. To understand why this is the case, it can be helpful to consider how different frequencies affect the kernel. A Fourier feature with zero frequency parameter is constant γ_0 , by definition. For $\omega' = \mathbf{0}$ we therefore have a constant Fourier feature for the non-stationary component $\gamma_{\omega'}(\mathbf{a}_v) = \gamma_0$ and a kernel that is solely defined in the filter space. If both $\omega = \omega' = \mathbf{0}$, we also have a constant Fourier feature for the non-stationary component $\gamma_\omega(\mathbf{a}_{v^{-1}u}) = \gamma_0$ and a kernel that is constant everywhere, which results in invariant pooling. Positive values for ω' introduce non-stationarity that effectively relaxes the strict equivariance constraints of the convolution at $\omega' = \mathbf{0}$. Lastly, note that individual scalars in ω' correspond to particular subgroups and we can relax equivariance constraints of specific subgroups by letting ω' be greater than zero in the associated dimension.

Example for translation group Let us consider relaxing equivariance of the translation group $G = T(2)$, as an example. Since $\dim(T(2)) = 2$, we have a two dimensional filter space and domain space and therefore also two-dimensional filter space frequencies $\omega = [\omega_x, \omega_y]^T \in \mathbb{R}^2$ and two domain space frequencies $\omega' = [\omega'_x, \omega'_y]^T \in \mathbb{R}^2$. If $\omega' = [0, 0]^T$, the layer reduces to a translationally equivariant convolutional layer. In other words, for any value of ω or weights θ the kernel remains stationary (as we have $\omega' = \mathbf{0}$). In this case the layer equals a convolution where the same filter is applied to all locations in the input. Higher values of ω , i.e. $\omega_x, \omega_y > 0$, correspond to more rapid changes in x- and y-direction in filter space, but it remains the same filter signal that is applied independent of the input location. If, instead, we let the components of the domain space frequencies ω' become non-zero, i.e. $\omega'_x, \omega'_y > 0$, then the kernel values can also depend on the absolute coordinate in the input image. Higher ω' result in a more rapidly changing kernel relative to different absolute locations in the input image. This non-stationarity breaks equivariance constraints in a continuous way. For sufficiently high ω' , the function can become akin to a linear product that has enough variance to place an independent weight on each pixel location. In practice, this would also require a sufficiently flexible NN_θ to represent such function. An illustration of the different symmetry modes for translation $G = T(2)$ is shown in Fig. 1.

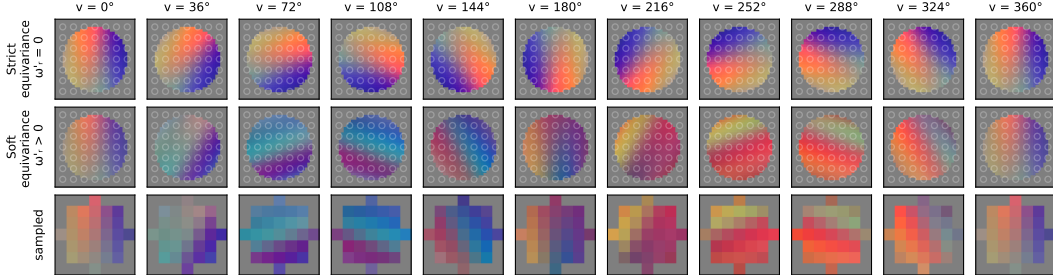


Figure 3: Equivariant and soft-equivariant $SO(2)$ filter banks. The top row shows a strict rotation equivariant filter bank for $\omega_r' = 0$. The middle row shows a filter bank with positive non-stationary frequencies $\omega_r' > 0$, without strict equivariance constraints. Sampled group elements at the bottom.

5 Implementation

Filter parameterisation and frequencies All models, including the $T(2)$ -equivariant and strict- $SE(2)$ equivariant baselines, follow the same architecture and settings as prior work by [24]. Importantly, all models use continuous kernels that are parameterised using Fourier basis features, which is common in literature. As all baselines use the same architectures, training settings and Fourier representations for the kernels, we can attribute gains in performance solely to the relaxation of equivariance.

To select ω , we use the same frequencies as used to initialise filter frequencies in [24]. To select ω' for the models with relaxed equivariance, we use cross-validation and limit the search space by considering equal frequencies along translational axes, ie. $\omega_x' = \omega_y'$, and share frequencies across layers. This scales the frequencies along the x- and y-axis equally in the Fourier basis, but does not constrain the kernel itself to be isotropic. Independent frequencies per layer is interesting future work. Lastly, to ensure the kernel is smooth in $SO(2)$, we let ω_r , ω_r' and associated entries in W be integer valued, similar to circular harmonics. An overview of the components in ω and ω' for different groups can be found in Table 1.

Sampling. The integral in Eq. (2) is not tractable in closed form and we therefore choose to approximate it by using samples, similar to Finzi et al. [7]. We deterministically evaluate group elements in $T(2)$ that correspond to (lifted) pixel locations and randomly sample 4, 8 or 16 group elements uniformly over $SO(2)$. For [24], the uniform distribution over $SO(2)$ covers the entire group at the start of training but has an adjustable range that is learned by early-stopping on the validation loss. All models used in the experiments use continuously parameterised kernels.

Locally-supported in filter space. Similar to conventional convolutional networks, we only define the kernel in a local subset S of the filter space, forcing the kernel to be zero $k_\theta = 0$ outside this local support. Doing so, makes the approximation of the integral in Eq. (2) much cheaper as we only need to sample the group elements within the support. Another consequence is that we no longer obtain strictly invariant global-pooling of Eq. (5). Instead, a kernel that is only a constant non-zero value in a local support represents a local-pooling layer, where the pool size equals the support size. In the experiments we let S be a disk in $T(2)$ with a diameter equal to 7 pixels in the input domain \mathcal{X} .

Table 1: Summary of used frequency parameters for particular symmetry constraints.

Model		$T(2)$	$SO(2)$	ω	ω'
$T(2)$ -CNN (regular continuous CNN)		strict	-	ω_x, ω_y	
$SE(2)$ -CNN		strict	strict	$\omega_x, \omega_y, \omega_r$	
soft $T(2)$ -CNN	(ours)	soft	-	ω_x, ω_y	ω_x', ω_y'
soft $SE(2)$ -CNN [soft in $SO(2)$]	(ours)	strict	soft	$\omega_x, \omega_y, \omega_r$	ω_r'
soft $SE(2)$ -CNN [soft in $T(2)$]	(ours)	soft	strict	$\omega_x, \omega_y, \omega_r$	ω_x', ω_y'
soft $SE(2)$ -CNN [soft in $T(2)$ and $SO(2)$]	(ours)	soft	soft	$\omega_x, \omega_y, \omega_r$	$\omega_x', \omega_y', \omega_r'$

Table 2: Image classification test accuracies. Comparison between strict and relaxed equivariant models. Mean and standard error $\frac{\sigma}{\sqrt{3}}$ are reported over three different random seeds.

Group	No. samples in $SO(2)$	$T(2)$ \times $SO(2)$		Model	Test accuracy			
					CIFAR-10		CIFAR-100	
					no augment	+ augment	no augment	+ augment
$T(2)$	1	Strict	-	CNN	81.80 \pm 0.48	85.87 \pm 0.22	46.20 \pm 0.09	53.97 \pm 0.33
		Soft	-	Ours	81.82 \pm 0.18	87.74 \pm 0.13	46.84 \pm 0.19	58.12 \pm 0.31
$SE(2)$ $= T(2) \times SO(2)$	4	Strict	Strict	G-CNN	81.39 \pm 0.26	85.76 \pm 0.21	44.00 \pm 0.18	49.81 \pm 0.56
		Strict	Partial	Romero and Lohit [24]	83.04 \pm 0.25	84.26 \pm 0.55	46.69 \pm 1.02	52.67 \pm 0.40
		Strict	Soft	Ours	83.21 \pm 0.03	87.02 \pm 0.22	49.47 \pm 0.41	54.48 \pm 0.27
	8	Strict	Strict	G-CNN	82.16 \pm 0.26	87.48 \pm 0.06	46.43 \pm 0.14	54.07 \pm 0.19
		Strict	Partial	Romero and Lohit [24]	84.82 \pm 0.20	87.37 \pm 0.61	51.04 \pm 0.61	58.22 \pm 0.25
		Strict	Soft	Ours	86.39 \pm 0.15	88.38 \pm 0.34	54.68 \pm 0.49	60.83 \pm 0.43
16	Strict	Strict	G-CNN	83.33 \pm 0.13	87.15 \pm 0.02	47.68 \pm 0.15	54.20 \pm 0.21	
	Strict	Partial	Romero and Lohit [24]	85.92 \pm 0.32	89.48 \pm 0.41	50.58 \pm 0.49	59.63 \pm 0.27	
	Strict	Soft	Ours	86.29 \pm 0.29	89.65 \pm 0.22	54.50 \pm 0.26	60.27 \pm 0.31	

6 Experiments

6.1 Verifying soft-equivariance using symmetry misspecification toy example

To verify that relaxed equivariance allows for less restrictive functions compared to strict equivariance, we repeat the MNIST6-180 problem of [24] and include our model. This toy problem is designed such that it can not be solved under strict symmetry constraints. It consists of the 6’s in the MNIST dataset with half of the dataset randomly rotated by 180° degrees. The task is to determine whether a sample has been rotated, i.e., a binary classification problem between ‘6’s and ‘9’s. In Table 3, we compare a rotation invariant G-CNN model that consists of multiple strictly equivariant layers followed by group pooling and compare with [24] and our model. In line with our expectations, we find that in this artificial set-up the relaxed ResNet model quickly converges to 100% test accuracy. The model with strict rotation symmetry is unable to distinguish between ‘6’s and ‘9’s and can thus not improve over a simple coin-flip with 50% accuracy on average.

Table 3: Toy problem. Models that obey strict rotation symmetry can not distinguish between 6’s and 9’s whereas the task can be solved under relaxed symmetry constraints.

$SO(2)$	Model	Test accuracy MNIST6-180
Strict	G-CNN	50.0
	Sparse [24]	100.0
Relaxed	Soft (ours)	100.0

6.2 Evaluating different fixed levels of relaxed equivariance

We assess the effectivity of relaxing equivariance constraints for translation and rotation groups $T(2)$, $SO(2)$ and $SE(2)$ on CIFAR-10 and CIFAR-100 image classification tasks. As strict symmetries can lead to misspecification, we hypothesise that relaxed equivariance can improve the model performance on these tasks. As baselines, we use a strictly equivariant G-CNNs and a Partial G-CNNs [24]. The difference in model sizes arising from different kernel input dimensions are neglectable compared to the total number of model parameters for the used architecture. In Fig. 4, we plot performance on the validation set for different values of frequency parameter ω' and list final test accuracies in Table 2. From Table 2, we can see that our method outperforms the baseline on both datasets across all settings. This holds both with and without data augmentation, showing that the benefit of relaxed equivariance does not disappear when using augmentations. On $T(2)$, we find that the improvement is negligible small and it would be interesting to see whether this gap becomes larger with increased number of basis functions or other choices of NN_θ . We observe particularly large improvements in test accuracy for soft- $SO(2)$ on CIFAR-10 and CIFAR-100. On CIFAR-100, relaxing equivariance improves test accuracy of the non-invariant baseline by 6 percentage points when using augmentation and improves by 8 percentage, without augmentation.

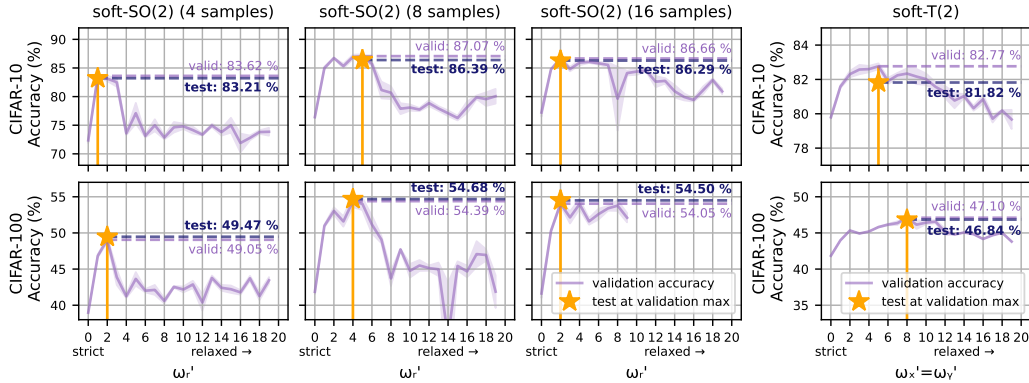


Figure 4: Relaxing equivariance constraints. Test accuracy on CIFAR-10 and CIFAR-100 is shown for SE(2)-equivariant models with soft-SO(2) equivariances for different values of ω'_r and soft-T(2) equivariance varying $\omega'_x = \omega'_y$. Some relaxation increases test accuracy in all cases, but the benefits diminish when relaxed too much. We use cross-validation to find the optimal relaxation and find that this outperforms strict equivariance constraints in all cases.

To further assess the effect of equivariance relaxation has on model performance, we can examine the impact different values for of non-stationary frequency parameter ω' on model performance. In Fig. 4, we show validation accuracy for different ω' averaged over three seeds with error bars corresponding to standard error ($\frac{\sigma}{\sqrt{3}}$) and show final test accuracy for model with best validation score. The scale of the x-axis should not directly be interpret as this depends on the chosen basis, parameterisation and initialisation of NN_θ . We observe that some relaxation of equivariance with frequency parameter $\omega' \neq \mathbf{0}$ leads to better test accuracy compared to the strict equivariant model at $\omega' = \mathbf{0}$. The benefits of the relaxation diminishes when equivariance is further relaxed. This is to be expected, as this then corresponds to very high frequencies in domain space which are unlikely to provide useful features anymore. We find that there exists an optimal amount of relaxation, which we can find with cross-validation. In all cases, we find that sufficiently relaxing equivariance results in higher test accuracy compared to strict equivariance. This indicates that strict equivariance might be slightly misspecified in this setting, to which our approach offers a solution.

6.3 Gradient-based learning of relaxed equivariance

Instead of using cross-validation, we also explore whether the right amount of equivariance can be learned using gradients. This is desirable, since cross-validation is an expensive procedure because model need to be retrained for different relaxations and requires additional hold-out validation data. Furthermore, finding the amount of equivariance using cross-validation may require sharing ω' across layers in practice to limit the search space to a single dimension, causing each layer to always have the same amount of relaxation. Training ω' with backpropagation, alongside the model parameters, is far from trivial as equivariance acts as a constraint on the functions a neural network can represent. Therefore, we can not expect that increased equivariance will lead to an improvement in terms of the regular (cross-entropy) training loss and be learned by directly optimising it with such loss. To learn equivariance constraints, which we expect will improve generalisation performance on test data, we propose to add a regularising term $\lambda \|\omega'\|_2^2$ to the objective, to encourage symmetry. The loss is inspired by the regularisation proposed in Augerino [4] to learn augmented inputs, and similarly requires an additional hyperparameter $\lambda \in \mathbb{R}$. From a Bayesian point of view, the new objective can be interpret as finding a maximum a posteriori probability (MAP) estimate after placing a Gaussian prior on the relaxation frequency parameter $\mathcal{N}(\omega' | \mathbf{0}, \frac{1}{2\lambda} \mathbf{I})$ (see App. B.2 for details).

In Table 4, we compare models with the partial and strict equivariance baselines, as well as the best fixed amount of equivariance found by cross-validation. We report the mean and standard error of the test accuracy on CIFAR-10 and CIFAR-100 over 3 seeds, trained with and without augmentation. For most settings of λ , the model achieves similar or improved performance over the best fixed settings found by cross-validated settings, outperforming the baselines with partial and strict equivariance. This is a promising result as it indicates that we can learn the amount of layer-wise equivariance as part of a single training procedure, without requiring expensive cross-validation or validation data.

Table 4: Learning the amount of equivariance with gradients. Comparison of soft $SE(2)$ relaxations where the amount of equivariance ω' is learned for different regularisation strengths λ . Equivariance learning achieves similar or improved test accuracy on CIFAR-10/CIFAR-100 tasks compared to the best value found by cross-validation, outperforming baselines with strict and partial equivariance.

Group	# samples in $SO(2)$	T(2)	$\times SO(2)$	Model	relaxation ω'	set by	Test accuracy			
							CIFAR-10		CIFAR-100	
							no augment	+ augment	no augment	+ augment
T(2)	1	Strict	-	CNN	-	-	81.80 \pm 0.48	85.87 \pm 0.22	46.20 \pm 0.09	53.97 \pm 0.33
		Soft	-	Ours	fixed ω'	(cross-validated)	81.82 \pm 0.18	87.74 \pm 0.13	46.84 \pm 0.19	58.12 \pm 0.31
		Soft	-	Ours	learned ω'	$\lambda=0.001$	79.99 \pm 0.22	87.04 \pm 0.17	46.21 \pm 0.20	55.46 \pm 0.11
		Soft	-	Ours	learned ω'	$\lambda=0.01$	82.04 \pm 0.16	87.28 \pm 0.17	46.45 \pm 0.15	56.32 \pm 0.35
		Soft	-	Ours	learned ω'	$\lambda=0.1$	82.10 \pm 0.07	87.33 \pm 0.18	46.55 \pm 0.07	56.40 \pm 0.08
		Soft	-	Ours	learned ω'	$\lambda=0.5$	82.20 \pm 0.17	87.58 \pm 0.06	46.92 \pm 0.12	56.32 \pm 0.12
		Soft	-	Ours	learned ω'	$\lambda=1.0$	81.89 \pm 0.21	87.25 \pm 0.06	46.82 \pm 0.10	56.80 \pm 0.09
		Soft	-	Ours	learned ω'	$\lambda=5.0$	81.60 \pm 0.13	87.35 \pm 0.11	47.00 \pm 0.07	57.02 \pm 0.24
		$SE(2)$ $=T(2)\times SO(2)$	4	Strict	Strict	G-CNN	-	-	81.39 \pm 0.26	85.76 \pm 0.21
Strict	Partial			Romero and Lohit [24]	-	-	83.04 \pm 0.25	84.26 \pm 0.55	46.69 \pm 1.02	52.67 \pm 0.40
Strict	Soft			Ours	fixed ω'	(cross-validated)	83.21 \pm 0.03	87.02 \pm 0.22	49.47 \pm 0.41	54.48 \pm 0.27
Strict	Soft			Ours	learned ω'	$\lambda=0.001$	81.19 \pm 0.16	83.51 \pm 0.23	46.67 \pm 0.37	51.51 \pm 0.40
Strict	Soft			Ours	learned ω'	$\lambda=0.01$	80.44 \pm 0.02	83.54 \pm 0.26	46.85 \pm 0.33	51.96 \pm 0.16
Strict	Soft			Ours	learned ω'	$\lambda=0.1$	83.70 \pm 0.16	86.29 \pm 0.35	49.14 \pm 0.42	55.70 \pm 1.18
Strict	Soft			Ours	learned ω'	$\lambda=0.5$	82.68 \pm 0.03	85.94 \pm 0.42	51.46 \pm 0.44	55.37 \pm 0.30
Strict	Soft			Ours	learned ω'	$\lambda=1.0$	82.66 \pm 0.53	85.18 \pm 0.47	51.34 \pm 0.44	55.97 \pm 0.93
Strict	Soft			Ours	learned ω'	$\lambda=5.0$	82.47 \pm 0.55	85.71 \pm 0.16	52.19 \pm 0.15	56.34 \pm 0.78
8	Strict		Strict	G-CNN	-	-	82.16 \pm 0.26	87.48 \pm 0.06	46.43 \pm 0.14	54.07 \pm 0.19
	Strict		Partial	Romero and Lohit [24]	-	-	84.82 \pm 0.20	87.37 \pm 0.61	51.04 \pm 0.61	58.22 \pm 0.25
	Strict		Soft	Ours	fixed ω'	(cross-validated)	86.39 \pm 0.15	88.38 \pm 0.34	54.68 \pm 0.49	60.83 \pm 0.43
	Strict		Soft	Ours	learned ω'	$\lambda=0.001$	83.54 \pm 0.09	86.99 \pm 0.39	50.14 \pm 0.16	56.29 \pm 0.27
	Strict		Soft	Ours	learned ω'	$\lambda=0.01$	83.27 \pm 0.23	87.10 \pm 0.06	50.56 \pm 0.48	56.48 \pm 0.50
	Strict		Soft	Ours	learned ω'	$\lambda=0.1$	86.36 \pm 0.09	89.26 \pm 0.10	54.41 \pm 0.39	60.94 \pm 0.28
	Strict		Soft	Ours	learned ω'	$\lambda=0.5$	86.06 \pm 0.10	88.64 \pm 0.37	57.11 \pm 0.23	60.67 \pm 0.29
	Strict		Soft	Ours	learned ω'	$\lambda=1.0$	85.71 \pm 0.34	88.90 \pm 0.06	56.28 \pm 0.11	60.95 \pm 0.65
	Strict		Soft	Ours	learned ω'	$\lambda=5.0$	85.91 \pm 0.19	88.51 \pm 0.12	56.25 \pm 0.26	60.45 \pm 0.18
16	Strict	Strict	G-CNN	-	-	83.33 \pm 0.13	87.15 \pm 0.02	47.68 \pm 0.15	54.20 \pm 0.21	
	Strict	Partial	Romero and Lohit [24]	-	-	85.92 \pm 0.32	89.48 \pm 0.41	50.58 \pm 0.49	59.63 \pm 0.27	
	Strict	Soft	Ours	fixed ω'	(cross-validated)	86.29 \pm 0.29	89.65 \pm 0.22	54.50 \pm 0.26	60.27 \pm 0.31	
	Strict	Soft	Ours	learned ω'	$\lambda=0.001$	83.39 \pm 0.12	87.87 \pm 0.27	49.24 \pm 0.55	57.22 \pm 0.18	
	Strict	Soft	Ours	learned ω'	$\lambda=0.01$	83.59 \pm 0.09	87.96 \pm 0.19	49.63 \pm 0.48	57.87 \pm 0.25	
	Strict	Soft	Ours	learned ω'	$\lambda=0.1$	85.81 \pm 0.16	89.69 \pm 0.18	55.11 \pm 0.15	62.22 \pm 0.23	
	Strict	Soft	Ours	learned ω'	$\lambda=0.5$	85.85 \pm 0.19	89.35 \pm 0.18	55.89 \pm 0.22	61.87 \pm 0.15	
	Strict	Soft	Ours	learned ω'	$\lambda=1.0$	85.74 \pm 0.24	89.47 \pm 0.10	55.21 \pm 0.13	61.08 \pm 0.23	
	Strict	Soft	Ours	learned ω'	$\lambda=5.0$	85.95 \pm 0.19	89.30 \pm 0.22	56.12 \pm 0.18	60.87 \pm 0.18	

7 Conclusion

In this work, we have proposed a generalisation of the group convolution that allows for a smooth parameter-efficient relaxation of otherwise strict symmetry constraints. The main idea is to use a non-stationary kernel that also depends on the absolute input group element, breaking strict equivariance constraints. Moreover, we show that we can obtain explicit control over the symmetry constraints through tunable frequency parameters, by representing group elements in a Fourier feature space.

We demonstrate relaxed equivariance in neural networks with roto-translation equivariance, relaxing the rotation and translation subgroups. We find that some relaxation of equivariance yield higher test accuracies on CIFAR-10 and CIFAR-100 image classification tasks, with and without augmentation. Furthermore, we show that the ω' parameter controlling the amount of equivariance can be learned with gradients from training data. Learning the amount of equivariance achieves similar or improved performance compared to the best value found by cross-validation and outperforms baselines with partial or strict equivariance. To perform gradient-based equivariance learning, we encourage symmetry using a similar regularisation as proposed in Augerino [4] to learn augmented inputs. Some limitations of directly regularising symmetry have been discussed in [12], such as the need for an additional hyperparameter that needs tuning and dependence on the used parameterisation of symmetry. It would be interesting to investigate whether alternative objectives [29, 33, 12] could resolve such issues. Symmetry discovery methods in literature often focus on invariances, which are easier to parameterise, whereas this work offers a way to parameterise learnable equivariance. This paves the way for automatic layer-by-layer symmetry discovery as part of a single training procedure.

By relaxing equivariance properties we can leverage useful inductive bias that symmetries can provide, while preventing possible symmetry misspecification if data does not fully obey an embedded symmetries. Experimentally, we have demonstrated that neural network layers with relaxed equivariance constraints can improve test accuracy on CIFAR-10 and CIFAR-100 image classification tasks, outperforming strict-equivariant models with up to 10 percentage points in test accuracy on CIFAR-100. We hope that the proposed non-stationary kernel as a general building block can be useful in machine learning applications that require smooth relaxations of symmetry constraints.

References

- [1] Ferran Alet, Dylan Doblar, Allan Zhou, Josh Tenenbaum, Kenji Kawaguchi, and Chelsea Finn. Noether networks: meta-learning useful conserved quantities. *Advances in Neural Information Processing Systems*, 34, 2021.
- [2] Ronen Basri, Meirav Galun, Amnon Geifman, David Jacobs, Yoni Kasten, and Shira Kritchman. Frequency bias in neural networks for input of non-uniform density. In *International Conference on Machine Learning*, pages 685–694. PMLR, 2020.
- [3] Erik J Bekkers, Maxime W Lafarge, Mitko Veta, Koen AJ Eppenhof, Josien PW Pluim, and Remco Duits. Roto-translation covariant convolutional networks for medical image analysis. In *International conference on medical image computing and computer-assisted intervention*, pages 440–448. Springer, 2018.
- [4] Gregory Benton, Marc Finzi, Pavel Izmailov, and Andrew Gordon Wilson. Learning invariances in neural networks. *arXiv preprint arXiv:2010.11882*, 2020.
- [5] Taco Cohen and Max Welling. Group equivariant convolutional networks. In *International conference on machine learning*, pages 2990–2999. PMLR, 2016.
- [6] Taco S Cohen, Mario Geiger, Jonas Köhler, and Max Welling. Spherical cnns. *arXiv preprint arXiv:1801.10130*, 2018.
- [7] Marc Finzi, Samuel Stanton, Pavel Izmailov, and Andrew Gordon Wilson. Generalizing convolutional neural networks for equivariance to lie groups on arbitrary continuous data. In *International Conference on Machine Learning*, pages 3165–3176. PMLR, 2020.
- [8] Marc Finzi, Gregory Benton, and Andrew G Wilson. Residual pathway priors for soft equivariance constraints. *Advances in Neural Information Processing Systems*, 34, 2021.
- [9] Marc Finzi, Max Welling, and Andrew Gordon Wilson. A practical method for constructing equivariant multilayer perceptrons for arbitrary matrix groups. In *International Conference on Machine Learning*, pages 3318–3328. PMLR, 2021.
- [10] Fabian Fuchs, Daniel Worrall, Volker Fischer, and Max Welling. Se (3)-transformers: 3d roto-translation equivariant attention networks. *Advances in Neural Information Processing Systems*, 33:1970–1981, 2020.
- [11] Kaiming He, Xiangyu Zhang, Shaoqing Ren, and Jian Sun. Deep residual learning for image recognition. In *Proceedings of the IEEE conference on computer vision and pattern recognition*, pages 770–778, 2016.
- [12] Alexander Immer, Tycho F. A. van der Ouderaa, Vincent Fortuin, Gunnar Rätsch, and Mark van der Wilk. Invariance learning in deep neural networks with differentiable laplace approximations, 2022.
- [13] Sergey Ioffe and Christian Szegedy. Batch normalization: Accelerating deep network training by reducing internal covariate shift. In *International conference on machine learning*, pages 448–456. PMLR, 2015.
- [14] David M Knigge, David W Romero, and Erik J Bekkers. Exploiting redundancy: Separable group convolutional networks on lie groups. In *International Conference on Machine Learning*, pages 11359–11386. PMLR, 2022.
- [15] Risi Kondor and Shubhendu Trivedi. On the generalization of equivariance and convolution in neural networks to the action of compact groups. In *International Conference on Machine Learning*, pages 2747–2755. PMLR, 2018.
- [16] Risi Kondor, Zhen Lin, and Shubhendu Trivedi. Clebsch–gordan nets: a fully fourier space spherical convolutional neural network. *Advances in Neural Information Processing Systems*, 31:10117–10126, 2018.
- [17] Rosanne Liu, Joel Lehman, Piero Molino, Felipe Petroski Such, Eric Frank, Alex Sergeev, and Jason Yosinski. An intriguing failing of convolutional neural networks and the coordconv solution. *arXiv preprint arXiv:1807.03247*, 2018.
- [18] Jonathan Lorraine, Paul Vicol, and David Duvenaud. Optimizing millions of hyperparameters by implicit differentiation. In Silvia Chiappa and Roberto Calandra, editors, *Proceedings of the Twenty Third International Conference on Artificial Intelligence and Statistics*, volume 108 of *Proceedings of Machine Learning Research*, pages 1540–1552. PMLR, 26–28 Aug 2020.

- [19] Gary F Margrave. Theory of nonstationary linear filtering in the fourier domain with application to time-variant filtering. *Geophysics*, 63(1):244–259, 1998.
- [20] Ben Mildenhall, Pratul P. Srinivasan, Matthew Tancik, Jonathan T. Barron, Ravi Ramamoorthi, and Ren Ng. Nerf: Representing scenes as neural radiance fields for view synthesis. In *ECCV*, 2020.
- [21] Adam Paszke, Sam Gross, Soumith Chintala, Gregory Chanan, Edward Yang, Zachary DeVito, Zeming Lin, Alban Desmaison, Luca Antiga, and Adam Lerer. Automatic differentiation in pytorch. 2017.
- [22] Nasim Rahaman, Aristide Baratin, Devansh Arpit, Felix Draxler, Min Lin, Fred Hamprecht, Yoshua Bengio, and Aaron Courville. On the spectral bias of neural networks. In *International Conference on Machine Learning*, pages 5301–5310. PMLR, 2019.
- [23] Ali Rahimi, Benjamin Recht, et al. Random features for large-scale kernel machines. In *NIPS*. Citeseer, 2007.
- [24] David W Romero and Suhas Lohit. Learning equivariances and partial equivariances from data. *arXiv preprint arXiv:2110.10211*, 2021.
- [25] David W Romero, Robert-Jan Bruijntjes, Jakub M Tomczak, Erik J Bekkers, Mark Hoogendoorn, and Jan C van Gemert. Flexconv: Continuous kernel convolutions with differentiable kernel sizes. *arXiv preprint arXiv:2110.08059*, 2021.
- [26] David W Romero, Anna Kuzina, Erik J Bekkers, Jakub M Tomczak, and Mark Hoogendoorn. Ckconv: Continuous kernel convolution for sequential data. *arXiv preprint arXiv:2102.02611*, 2021.
- [27] Victor Garcia Satorras, Emiel Hoogeboom, and Max Welling. E (n) equivariant graph neural networks. In *International Conference on Machine Learning*, pages 9323–9332. PMLR, 2021.
- [28] Kristof Schütt, Pieter-Jan Kindermans, Huziel Enoc Saucedo Felix, Stefan Chmiela, Alexandre Tkatchenko, and Klaus-Robert Müller. Schnet: A continuous-filter convolutional neural network for modeling quantum interactions. *Advances in neural information processing systems*, 30, 2017.
- [29] Pola Schwöbel, Martin Jørgensen, Sebastian W Ober, and Mark van der Wilk. Last layer marginal likelihood for invariance learning. *arXiv preprint arXiv:2106.07512*, 2021.
- [30] Vincent Sitzmann, Julien Martel, Alexander Bergman, David Lindell, and Gordon Wetzstein. Implicit neural representations with periodic activation functions. *Advances in Neural Information Processing Systems*, 33, 2020.
- [31] Danica J Sutherland and Jeff Schneider. On the error of random fourier features. *arXiv preprint arXiv:1506.02785*, 2015.
- [32] Matthew Tancik, Pratul P Srinivasan, Ben Mildenhall, Sara Fridovich-Keil, Nithin Raghavan, Utkarsh Singhal, Ravi Ramamoorthi, Jonathan T Barron, and Ren Ng. Fourier features let networks learn high frequency functions in low dimensional domains. *arXiv preprint arXiv:2006.10739*, 2020.
- [33] Tycho FA van der Ouderaa and Mark van der Wilk. Learning invariant weights in neural networks. In *Workshop in Uncertainty & Robustness in Deep Learning, ICML*, 2021.
- [34] Mark van der Wilk, Matthias Bauer, ST John, and James Hensman. Learning invariances using the marginal likelihood. *arXiv preprint arXiv:1808.05563*, 2018.
- [35] Rui Wang, Robin Walters, and Rose Yu. Approximately equivariant networks for imperfectly symmetric dynamics. *arXiv preprint arXiv:2201.11969*, 2022.
- [36] Maurice Weiler, Mario Geiger, Max Welling, Wouter Boomsma, and Taco Cohen. 3d steerable cnns: Learning rotationally equivariant features in volumetric data. *arXiv preprint arXiv:1807.02547*, 2018.
- [37] Daniel E Worrall and Max Welling. Deep scale-spaces: Equivariance over scale. *arXiv preprint arXiv:1905.11697*, 2019.
- [38] Daniel E Worrall, Stephan J Garbin, Daniyar Turmukhambetov, and Gabriel J Brostow. Harmonic networks: Deep translation and rotation equivariance. In *Proceedings of the IEEE Conference on Computer Vision and Pattern Recognition*, pages 5028–5037, 2017.

- [39] Manzil Zaheer, Satwik Kottur, Siamak Ravanbakhsh, Barnabas Poczos, Ruslan Salakhutdinov, and Alexander Smola. Deep sets. *arXiv preprint arXiv:1703.06114*, 2017.
- [40] Allan Zhou, Tom Knowles, and Chelsea Finn. Meta-learning symmetries by reparameterization. *arXiv preprint arXiv:2007.02933*, 2020.

Checklist

1. For all authors...
 - (a) Do the main claims made in the abstract and introduction accurately reflect the paper's contributions and scope? [Yes]
 - (b) Did you describe the limitations of your work? [Yes]
 - (c) Did you discuss any potential negative societal impacts of your work? [No]
 - (d) Have you read the ethics review guidelines and ensured that your paper conforms to them? [Yes]
2. If you are including theoretical results...
 - (a) Did you state the full set of assumptions of all theoretical results? [Yes]
 - (b) Did you include complete proofs of all theoretical results? [Yes]
3. If you ran experiments...
 - (a) Did you include the code, data, and instructions needed to reproduce the main experimental results (either in the supplemental material or as a URL)? [No] Used datasets are public and instructions can be found in the paper. However, the code is not yet publicly available.
 - (b) Did you specify all the training details (e.g., data splits, hyperparameters, how they were chosen)? [Yes]
 - (c) Did you report error bars (e.g., with respect to the random seed after running experiments multiple times)? [Yes]
 - (d) Did you include the total amount of compute and the type of resources used (e.g., type of GPUs, internal cluster, or cloud provider)? [No]
4. If you are using existing assets (e.g., code, data, models) or curating/releasing new assets...
 - (a) If your work uses existing assets, did you cite the creators? [Yes]
 - (b) Did you mention the license of the assets? [N/A]
 - (c) Did you include any new assets either in the supplemental material or as a URL? [N/A]
 - (d) Did you discuss whether and how consent was obtained from people whose data you're using/curating? [N/A]
 - (e) Did you discuss whether the data you are using/curating contains personally identifiable information or offensive content? [N/A]
5. If you used crowdsourcing or conducted research with human subjects...
 - (a) Did you include the full text of instructions given to participants and screenshots, if applicable? [N/A]
 - (b) Did you describe any potential participant risks, with links to Institutional Review Board (IRB) approvals, if applicable? [N/A]
 - (c) Did you include the estimated hourly wage paid to participants and the total amount spent on participant compensation? [N/A]

A Training details

A.1 Network architecture

In all experiments, we use the same architecture and training settings as prior work by [24]. The used architectures have a similar number of parameters within a 4% difference (see Table 5).

The architecture consists of a simple ResNet model [11]. A complete overview of the used architecture can be found in Sec. 5 and Fig. 3 of [24]. The network consists of a lifting layer, followed by two residual blocks with spatial max-pooling using a kernel size 2 after each group equivariant layer. After the last block, max pooling is applied over spatial and subgroup dimensions, followed by two linear layers with batch norm [13] and ReLU non-linearities.

A.2 On kernel parameterisations

Continuous parameterisations of convolutional kernels in the context of neural networks were first proposed in [28], but require less flexible isotropic kernels. Continuously parameterised kernels with more flexible MLPs were proposed in [9], using Swish activation functions. Later works [26, 24] showed that SIRENs [30], which use a random Fourier feature basis by effectively replacing Swish activation functions with sinusoidal activations, greatly improved performance.

Random Fourier features were originally proposed in [23] to approximate (exact in the infinite-width limit) the feature basis of the radial basis function [23]. Random Fourier features are well-known and widely used within machine learning. In a Deep Learning context, they can help to overcome spectral bias and can be an effective basis when learning complex continuous signals [32, 20]. For kernel parameterisations, this encompasses kernels parameterised by small MLPs with sinusoidal activation functions in the first layer, such as SIRENs [30]. In our case, we use a shallow MLP with 32 hidden units and cosine activation functions for $\text{NN}(\cdot)$, such that the continuous kernels are the same 3-layer SIREN as used in [24].

An ablation study of different activation functions for the architecture used in this study can be found in Table 4 of Appendix F in [24]. For a more complete overview, we refer to [26] for an ablation study for regular convolutional kernels, [24] for group convolutional kernels and partial equivariant kernels, and [14] for (separable) for group convolutional kernels. We use the same Fourier feature parameterisation in all models to parameterise continuous kernels.

A.3 Training settings

For the CIFAR-10 and CIFAR-100 datasets, we use the default train, validation and test split. We use a mini-batch size of 64 in all experiments. We optimise for 300 epochs with Adam ($\beta_1=0.9, \beta_2=0.999$) with a learning rate of 0.001, cosine annealed to zero with 5 epochs of linear warm-up and a weight decay of 0.0001.

A.4 Model parameter counts

For the strict and partial equivariant baselines, we use the same architecture as used in [24]. As can be seen from Table 5 reporting exact parameter counts, the models that were compared have approximately the same parameter counts.

Table 5: Number of parameters for different models.

Group	T(2)	\times SO(2)	Model	Parameter count	
				CIFAR-10	CIFAR-100
T(2)	Strict	-	CNN	451898	457748
	Soft	-	Ours	452282	458132
SE(2) = T(2) \times SO(2)	Strict	Strict	G-CNN	451898	457748
	Strict	Partial	Romero and Lohit [24]	469615	475465
	Strict	Soft	Ours	469802	475652

A.5 Runtimes

In Table 6, we report training and inference runtimes of our own implementation. Do note that these results are hardware and implementation specific. We used pytorch [21], which allows models to be efficiently run on an NVIDIA RTX 3090 24gb GPU. Adding strict rotational equivariance (SE(2) = T(2) \times SO(2)) is slower than only using T(2) equivariance, as it requires an extra dimension in the feature maps for samples of the rotation subgroup. Relaxing equivariance T(2) \times soft-SO(2), on the other hand, only requires an extra dependency in the kernel and does not come with an added computational cost. In this case, we show that relaxing equivariance can increase performance without an increase in train or inference time. We hypothesize that further engineering efforts, such as dedicated low-level CUDA implementations for (relaxed) convolutional operations, could further improve runtime performance.

Table 6: Overview of training and inference runtimes. We report the average runtime per mini-batch in seconds. Measured on CIFAR-10 on an NVIDIA RTX 3090 24 gb GPU.

Group	No. samples in SO(2)	T(2)	\times SO(2)	Model	Avg. runtime	
					Train	Inference
T(2)	1	Strict	-	CNN	3.5	0.2
		Soft	-	Ours	20.9	1.0
SE(2) = T(2) \times SO(2)	4	Strict	Strict	G-CNN	12.0	0.6
		Strict	Partial	Romero and Lohit [24]	12.1	0.6
		Strict	Soft	Ours	12.2	0.6
	8	Strict	Strict	G-CNN	29.1	1.3
		Strict	Partial	Romero and Lohit [24]	29.9	1.4
		Strict	Soft	Ours	29.4	1.4
	16	Strict	Strict	G-CNN	85.8	3.7
		Strict	Partial	Romero and Lohit [24]	86.9	3.8
		Strict	Soft	Ours	86.4	3.7

B Mathematical details

B.1 Relaxed kernel inputs $(v^{-1}u, u)$ and $(v^{-1}u, v)$ equally expressive as more general (u, v)

To relax the convolution operator, we let the kernel not only depend on $v^{-1}u$ but on also directly on the input group element v or output group element u : $k_1(v^{-1}u, u)$ or $k_2(v^{-1}u, v)$. We choose this form, as it allows us to parameterise the kernel in a way that can efficiently interpolate to convolutional kernels by letting it solely depend on the first argument $(v^{-1}u)$. We could consider writing our relaxed kernel in a more general form $k(u, v)$. However, upon a change-of-variables, this general form is just as expressive as the relaxed kernel in the sense that they can describe the same class of functions. To show this, we consider the reparameterisation $k = k_1 \circ f_1$ or $k = k_2 \circ f_2$. It suffices to show that bijections exist $f_1 : (a, b) \mapsto (b^{-1}a, a)$ and $f_2 : (a, b) \mapsto (b^{-1}a, b)$ between the forms:

$$(v^{-1}u, u) \xrightleftharpoons[f_1^{-1}]{f_1} (u, v) \xrightleftharpoons[f_2^{-1}]{f_2} (v^{-1}u, v)$$

If we choose inverse $f_1^{-1} : (a, b) \mapsto (b, ba^{-1})$ and $f_2^{-1} : (a, b) \mapsto (ba, b)$, it follows that

$$\begin{aligned} f_1^{-1}(v^{-1}u, u) &= (u, u(v^{-1}u)^{-1}) = (u, u(u^{-1}v)) = (u, (uu^{-1})v) = (u, v) \\ f_2^{-1}(v^{-1}u, v) &= (v(v^{-1}u), v) = ((vv^{-1})u, v) = (u, v) \end{aligned}$$

This confirms the bijection and we conclude that kernels that depend on (u, v) do, as such, not represent a broader function class than kernels that depend on $(v^{-1}u, u)$ or $(v^{-1}u, v)$. Observe that no such bijections can be found to $(v^{-1}u)$, as convolutional kernels are less expressive.

B.2 Bayesian interpretation of symmetry regularisation.

Similar to Augerino [4], we propose to encourage symmetry through an additional regularisation term $\lambda \|\omega'\|_2^2$ in the training objective. From a probabilistic perspective, this objective can be interpret as finding the maximum a posteriori probability (MAP) estimate after placing a Gaussian prior $\mathcal{N}(\omega' | \mathbf{0}, \frac{1}{2\lambda} \mathbf{I})$ on the frequency parameters ω' that control the amount of equivariance. The $\lambda \in \mathbb{R}$ hyperparameter is inversely proportional to the prior variance over relaxation parameter ω' . Note that $\omega' = \mathbf{0}$ corresponds to strict equivariance. Hence, high values of λ correspond to more strict equivariance whereas lower values lead to more relaxed constraints. The MAP estimate becomes:

$$\begin{aligned} \arg \max_{\theta, \omega'} p(\theta, \omega' | \mathcal{D}) &= \arg \max_{\theta, \omega'} [\log p(\mathcal{D} | \theta, \omega') + \log p(\omega')] \\ &= \arg \max_{\theta, \omega'} \left[\prod_{n=1}^N \log p(x_n | \theta, \omega') + \log \mathcal{N}(\omega' | \mathbf{0}, \frac{1}{2\lambda} \mathbf{I}) \right] \\ &= \arg \max_{\theta, \omega'} \left[\log \sum_{n=1}^N p(x_n | \theta, \omega') - \lambda (\omega')^T \omega' \right]. \end{aligned}$$

In other words, the loss that we minimise with respect to θ and ω' is:

$$\mathcal{L}_{\text{MAP}} = \underbrace{-\log \sum_{n=1}^N p(x_n | \theta, \omega')}_{\text{negative log likelihood / cross-entropy}} + \underbrace{\lambda \|\omega'\|_2^2}_{\text{symmetry regulariser}}$$

the sum of the cross-entropy commonly used in classification and the additional regulariser $\lambda \|\omega'\|_2^2$. From the prior, we can intuitively see why increasing λ encourages equivariance constraints. In the limit of infinite precision $\lambda \rightarrow \infty$, we have that the prior on the frequency components converges to a Dirac delta around zero and therefore always $\omega' = \mathbf{0}$: the setting in which we obtain strict equivariance.